Chemistry of Metals and Alloys

Chem. Met. Alloys 7 (2014) 85-99
Ivan Franko National University of Lviv
www.chemetal-journal.org

$Yb_2Al_{15}Pt_6$ – the most ordered variety of the $Sc_{1.2}Fe_4Si_{9.8}$ aristotype

Yurii PROTS[1*], Micha DEPPE[1], Raul CARDOSO-GIL[1], Antonio CERVELLINO[2], Alim ORMECI[1], Christoph GEIBEL[1], Yuri GRIN[1]

[1] *Max-Planck-Institut für Chemische Physik fester Stoffe, Nöthnitzer Str. 40, 01187 Dresden, Germany*
[2] *Paul Scherrer Institut, 5232 Villigen, Switzerland*
** Corresponding author. Tel.: +49-351-4646223; fax: +49-351-46464002; e-mail: prots@cpfs.mpg.de*

Dedicated to Evgen I. Gladyshevskii (1924-2012)

Received January 28, 2014; accepted June 26, 2014; available on-line November 10, 2014

The title compound was synthesized by reaction of the elemental components in a corundum crucible at 1450 ºC, and subsequent crystal growth using the Bridgman technique. The crystal structure of $Yb_2Al_{15}Pt_6$ was determined from X-ray single crystal diffraction data: space group *Cmcm*, Pearson symbol *oS*92, a = 12.7969(1) Å, b = 7.38813(7) Å, c = 16.3605(2) Å, R_F = 0.036 for 1455 observed structure factors and 65 variable parameters. The title compound crystallizes in a new type of structure, which represents an ordered variety of the $Sc_{1.2}Fe_4Si_{9.8}$ aristotype. The structure can be described as an $(ABB)_2$ stacking of two trigonal layers with compositions Yb_4Al_6 (*A*) and Pt_6Al_{12} (*B*). The layers *A* are almost planar and consist of ytterbium atoms arranged at the apexes of condensed hexagons centered by triangular Al_3 units. The slabs *B* may be considered as distorted hexagonal close-packed, similar to three adjacent layers I–Cd–I of the structure type CdI_2 (Al–Pt–Al). The structural particularities of $Yb_2Al_{15}Pt_6$ are discussed in comparison with the related structures of $Y_2Ga_9Co_3$, $Tb_2Ge_3Pt_9$, $Yb_2Ga_9Pd_3$ and $Er_4Al_{24}Pt_9$. A real-space analysis of the chemical bonding with the electron-localizability approach showed that the crystal structure of $Yb_2Al_{15}Pt_6$ consists of an anionic Al–Pt framework, with Yb cations embedded in cavities. The Al–Pt interactions within the framework are covalent polar, whereas ionic bonding is observed between ytterbium and the framework.

Ytterbium / Platinum / Aluminum / Crystal structure / Intermetallic compound

Introduction

Recently a series of ternary compounds of platinum and aluminum with the ideal composition $RE_2Pt_6Al_{15}$, containing Y, Zr and small rare-earth elements (Gd–Tm) as *RE* component [1-4], were reported to crystallize in a hexagonal structure first determined for $Sc_{1.2}Fe_4Si_{9.8}$ (space group $P6_3/mmc$, a = 3.897 Å, c = 15.160 Å) [5]. Starting from $Y_2Co_3Ga_9$ [6], several related structure types are described as stacking of two different pseudo-trigonal slabs with compositions RE_2M_3 (hereafter designated as *A*) and T_3M_6 (*B*, Fig. 1), where *T* corresponds to a transition metal and *M* to a main group element [6,7]. The sequence of the slabs in $Sc_{1.2}Fe_4Si_{9.8}$ and $RE_2Pt_6Al_{15}$ is $(ABB)_2$. Slab *B* may be considered as distorted hexagonal closest packed (Fig. 1, top), similar to a combination of three adjacent layers I–Cd–I of the CdI_2 structure type. Slab *A* is a planar layer. Both crystallographic positions, 2*d* and 6*h*, within this layer are usually described in the $Sc_{1.2}Fe_4Si_{9.8}$ type structures as partially occupied, typically with occupancy factors of ~⅔ and ~⅓ for the *RE* and *M* sites, respectively (Fig. 1, middle). The distances of ~1.5 Å between the atoms at these sites are too short to allow simultaneous occupation of both sites. Obviously, the structural model of the $Sc_{1.2}Fe_4Si_{9.8}$ type is averaged and does not reflect the real distribution of the atoms within the layer *A*. The simplest ordered description of the atoms within this layer requires an enlargement of the unit cell along [1-10], *i.e.* a √3 times larger lattice parameter a (Fig. 1, bottom) [1-3,8-12]. Numerous compounds with $Sc_{1.2}Fe_4Si_{9.8}$ structure type have been found with silicon, gallium and aluminum within the last three decades [1-5,8-20]. Even though different ordered varieties of the crystal structure have been proposed for these phases [1-3,8-12], none of these structure models has been found experimentally.

In this work we report the synthesis and growth of single crystals of the ternary compound $Yb_2Al_{15}Pt_6$, a hitherto missing member of the $RE_2Pt_6Al_{15}$ series [1]. The crystal structure of $Yb_2Al_{15}Pt_6$ is the first of the possible completely ordered varieties of the $Sc_{1.2}Fe_4Si_{9.8}$ aristotype. The results of an investigation of the physical properties of $Yb_2Al_{15}Pt_6$ (magnetic susceptibility $\chi(T)$, specific heat $C(T)$, resistivity $\rho(T)$

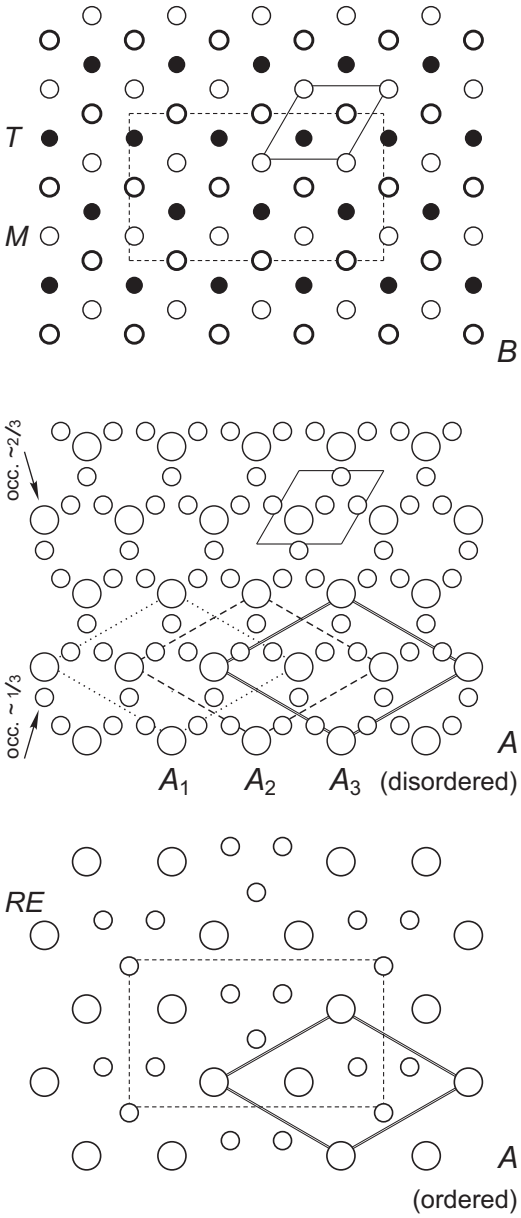

Fig. 1 Slabs *A* and *B* constituting the structures with $Sc_{1.2}Fe_4Si_{9.8}$ type subcell: (top) distorted hexagonal closest-packed slab *B* (solid line: $a_{subcell}$, dashed line: unit cell of $Yb_2Al_{15}Pt_6$); (middle) disorder in the slab *A* with partial occupations ~⅔ and ~⅓ for *RE* and *M* atoms, respectively; three different positions of an *A* slab with respect to the neighboring *B* slab are shown by dotted (*A*1), dashed (*A*2) and double (*A*3) lines; (bottom) ordered distribution of the atoms within the slab *A*, (double line: hexagonal cell with $a_{hex} = \sqrt{3}a_{subcell}$, dashed line: ortho-hexagonal unit cell of $Yb_2Al_{15}Pt_6$ with $a_{orth} = \sqrt{3}a_{hex} = \sqrt{3}\times\sqrt{3}a_{subcell} = 3a_{subcell}$ and $b_{orth} = a_{hex} = \sqrt{3}a_{subcell}$).

and thermoelectric power $S(T)$ measurements) are reported in a separate publication [21]. Preliminary results of this work were presented at a conference [22].

Experimental and calculation procedures

Single crystals of $Yb_2Al_{15}Pt_6$ were grown by the Bridgman technique. High-purity elements were used for the synthesis: Yb, 99.99 mass.%, Ames Laboratory, Pt, 99.9 mass.%, Heraeus, and Al, 99.999 mass.%, Alfa Aesar. Mixtures of small pieces of the components were put into corundum crucibles. The latter were enclosed into tantalum tubes of a small volume to prevent losses of Yb. The reaction charges were heated up to 1450 ºC and growth was started with a pulling rate of the order of 1–2 mm/h, equivalent to a temperature decrease of 1.6 ºC/h. Crystals were cleaved out from the batches and the surface was cleaned by polishing or cutting.

The composition of selected fragments of the crystals was studied by energy dispersive X-ray spectroscopy (EDXS), using a Philips XL30 scanning electron microscope, equipped with an EDAX Phoenix detector (Röntgenanalytik Messtechnik GmbH). As reference materials pure elements Yb, Pt and Al were used. Special care was taken to identify possible impurities in the EDX spectra.

Several fragments of the grown specimen were used for X-ray powder and single crystal investigations. The samples were first characterized by X-ray powder diffraction, using a Huber Guinier Imaging Plate Camera G670 (Cu $K\alpha_1$ radiation, λ = 1.54060 Å). High-resolution powder diffraction data (synchrotron radiation, λ = 0.495883 Å, calibrated by Si (NIST640c, a = 5.43119 Å), Mythen 2 microstrip detector [23], material science (MS) beam-line of the Synchrotron Lichtquelle Schweiz (SLS) at PSI, Villigen, Switzerland) were used for the analysis of possible reflection splitting, as well as for precise determination of the lattice parameters.

X-ray single crystal intensity data were collected on a Rigaku AFC7 automatic diffractometer, equipped with a Mercury CCD detector, using graphite-monochromated Mo $K\alpha$ radiation. The intensities of the reflections were corrected for absorption by the multi-scan routine [24]. Relevant crystallographic information and details of the data collection are listed in Table 1. The final positional parameters and the equivalent isotropic displacement parameters are given in Table 2. Interatomic distances are listed in Table 3.

For analysis of the powder patterns, the program package WinXPow was used [25]. Determination of the peak positions by profile fitting of their shape, indexing of the diffraction diagrams and lattice parameter refinement, as well as refinement of the crystal structure, were performed using the program package WinCSD [26]. Crystal structure solution was carried out with the program SHELXS86 [27]. The atomic parameters of the $Yb_2Al_{15}Pt_6$ structure were standardized using the program STRUCTURE TIDY [28,29].

Table 1 Crystallographic data for $Yb_2Al_{15}Pt_6$.

Composition	$Yb_2Al_{15}Pt_6$
Space group	*Cmcm* (no. 63)
Pearson symbol	*oS*92
Formula units per unit cell, *Z*	4
Lattice parameters [a] *a* / Å	12.7969(1)
b / Å	7.38813(7)
c / Å	16.3605(2)
V / Å^3	1546.8(1)
Calc. density / g cm^{-1}	8.25
Crystal form	prism-like
Crystal size / μm^3	25 × 30 × 70
Diffraction system	RIGAKU AFC7
Detector	Mercury CCD
Radiation, λ / Å	Mo $K\alpha$, 0.71073
Scan; step / degree; *N*(images)	φ; 0.6; 450
Maximal 2θ / degree	68.9
Range in *h*, *k*, *l*	$-10 \le h \le 16$, $-11 \le k \le 11$, $-26 \le l \le 19$
Absorption correction	multi-scan
T(max)/*T*(min)	1.68
Absorption coeff. / mm^{-1}	66.8
N(*hkl*) measured	5896
N(*hkl*) unique	1563
R_{int} [b]	0.035
N(*hkl*) observed	1455
Observation criteria	$F(hkl) \ge 4\sigma(F)$
Refined parameters	65
*R*1 ($F(hkl) > 4\sigma(F)$)	0.036
*wR*2 (all data)	0.073
Residual peaks / e Å^{-3}	–2.48/2.48

[a] Synchrotron data (PSI, SLS, MS beamline, λ = 0.495883 Å).

[b] The residuals are defined as follows $R_{int} = \Sigma(F_o^2 - F_o^2(\text{mean}))/\Sigma(F_o^2)$; $R(F) = \Sigma(|F_o| - |F_c|)/\Sigma|F_o|$; $wR(F^2) = \{\Sigma[w(F_o^2 - F_c^2)^2]/\Sigma[w(F_o^2)^2]\}^{1/2}$.

Table 2 Atomic coordinates and equivalent displacement parameters (in Å^2) in the crystal structure of $Yb_2Al_{15}Pt_6$.

Atom	Site	*x*	*y*	*z*	U_{eq}
Yb1 [a]	8*g*	0.16720(3)	0.33408(6)	¼	0.0085(1)
Pt1	16*h*	0.32896(2)	0.16228(4)	0.10945(2)	0.0067(1)
Pt2	8*f*	0	0.17534(5)	0.10838(2)	0.0068(1)
Al1	16*h*	0.1669(2)	0.3333(3)	0.0462(2)	0.0078(5)
Al2	16*h*	0.3365(2)	0.4974(3)	0.1359(2)	0.0088(4)
Al3	8*g*	0.3970(2)	0.2310(4)	¼	0.0090(6)
Al4	8*f*	0	0.1679(4)	0.5472(2)	0.0088(6)
Al5	8*f*	0	0.5048(4)	0.1366(2)	0.0086(6)
Al6	4*c*	0	0.0420(5)	¼	0.0081(8)

[a] The occupancy and atomic displacement parameters of Yb1 were constrained with Yb2 (4*c* site, 0 0.839(6) ¼) and resulted in an occupancy ratio of Yb1 : Yb2 = 0.987(2) : 0.013.

Table 3 Selected interatomic distances in the crystal structure of $Yb_2Al_{15}Pt_6$. All distances up to 4.20 Å, 4.20 Å and 3.60 Å in the coordination environments of the Yb, Pt and Al atoms, respectively, are listed.

Atoms		*d*, Å	Atoms		*d*, Å
Yb1 –	1Al3	3.038(3)	Al2 –	1Pt1	2.481(2)
	1Al6	3.039(3)		1Pt2	2.511(2)
	1Al3	3.045(3)		1Pt1	2.515(2)
	2Al5	3.100(2)		1Al3	2.821(3)
	2Al2	3.104(3)		1Al4	2.823(3)
	2Al2	3.111(3)		1Al5	2.823(2)
	2Al1	3.335(3)		1Al1	2.883(3)
	2Pt1	3.3429(4)		1Al1	2.887(3)
	2Pt1	3.3442(4)		1Yb1	3.105(2)
	2Pt2	3.3647(4)		1Yb1	3.111(3)
Pt1 –	1Al2	2.481(2)	Al3 –	2Pt1	2.511(1)
	1Al3	2.511(1)		1Al3	2.636(6)
	1Al2	2.515(2)		1Al6	2.649(4)
	1Al5	2.519(2)		2Al2	2.821(3)
	1Al1	2.547(3)		2Al5	2.823(4)
	1Al1	2.640(2)		1Yb1	3.038(3)
	1Al1	2.643(3)		1Yb1	3.045(3)
	1Al4	2.720(2)	Al4 –	1Pt2	2.547(3)
	1Yb1	3.3420(4)		2Pt1	2.720(2)
	1Yb1	3.3442(4)		1Pt2	2.726(3)
Pt2 –	1Al5	2.478(3)		2Al2	2.823(3)
	2Al2	2.511(2)		1Al5	2.825(4)
	1Al6	2.518(2)		2Al1	2.896(4)
	1Al4	2.547(3)		1Al4	2.923(6)
	2Al1	2.638(2)	Al5 –	1Pt2	2.478(3)
	1Al4	2.726(3)		2Pt1	2.518(2)
	2Yb1	3.3647(4)		2Al3	2.823(4)
Al1 –	1Pt1	2.547(3)		1Al4	2.825(4)
	1Pt2	2.638(2)		2Al1	2.891(3)
	1Pt1	2.640(2)		2Yb1	3.100(2)
	1Pt1	2.643(3)	Al6 –	2Pt2	2.518(2)
	1Al2	2.883(3)		2Al3	2.649(4)
	1Al1	2.885(4)		4Al2	2.823(2)
	1Al2	2.887(4)		2Yb1	3.039(3)
	1Al1	2.890(5)			
	1Al5	2.891(3)			
	1Al4	2.896(4)			
	1Yb1	3.335(3)			

The all-electron full-potential local orbital (FPLO) method [30] was used to investigate the electronic structure and chemical bonding of the title compound. Because the Yb 4*f* electrons give rise to states with narrow bandwidth, the local spin density approximation to the density functional theory had to be complemented by introducing an on-site Coulomb repulsion parameter *U* (LSDA+U method, [31]). Perdew-Wang parameterization [32] was employed for the LSDA part. The typical FPLO value $U = 8$ eV for the 4*f* electrons was applied [33]. With regard to the double-count correction scheme, the fully-localized limit (or atomic limit) method was chosen. Brillouin zone integrations were based on the linear tetrahedron method.

Real-space chemical bonding analysis was performed by combining topological analyses of the electron density and the electron localizability indicator (ELI), the so-called electron-localizability approach. The topological analysis of the electron density determines the regions in a molecule or crystal structure belonging to each atom, in accordance with Bader's quantum theory of atoms in molecules (QTAIM) [34]. Application of the same procedure to the ELI [35] provides information on atomic core regions and the nature of bonding in the valence region. In our study, the ELI was calculated in the ELI-D representation [36,37] using a module implemented in the FPLO package [38]. Topological analysis to find the attractors (local maxima of the ED or ELI-D), basins of attractors and the electron populations of the basins, was carried out by the program DGRID [39].

Results and discussion

Synthesis and crystal growth

Optimal conditions for the growth of $Yb_2Al_{15}Pt_6$ single crystals were achieved when an excess of about 7 at.% of Yb and 4 at.% of Pt was used. Besides well-developed single crystal specimens with average dimensions of about $0.7 \times 0.9 \times 3.5$ mm^3, the reaction mixture usually contained a small amount of microcrystalline binary phases: tetragonal Pt_8Al_{21} (own type) and cubic $PtAl_2$ (CaF_2 type). The crystals' composition obtained from the microprobe analyses agreed very well with those resulting from the crystal structure refinement. The ratio of the constituents (in at.%) in the single crystal specimen that was used for the structure investigation was $Yb : Pt : Al \approx 8.6(2) : 25.3(3) : 66.1(6)$, in good agreement with the ideal composition of 8.7 : 26.1 : 65.2. Further decrease of the amount of Yb in the starting reaction mixture resulted in degradation of the size of the crystals, as well as of their quality.

Powder diffraction characterization of the translation symmetry

Besides strong reflections matched with the unit cell of the $Sc_{1.2}Fe_4Si_{9.8}$ structure type ($a_{subcell} = 4.26$ Å, $c_{subcell} = 16.36$ Å), the powder diffraction pattern of $Yb_2Al_{15}Pt_6$ contains a set of relatively weak, but clearly recognizable peaks, which were indexed on the basis of a hexagonal unit cell with $a_{hex} = \sqrt{3}a_{subcell} = 7.38$ Å and $c_{hex} = c_{subcell} = 16.36$ Å (Fig. 2). The latter parameters are in good agreement with the ortho-hexagonal lattice parameters ($a_{orth} = \sqrt{3}a_{hex} = 12.79$ Å, $b_{orth} = b_{hex} = 7.38$ Å, $c_{orth} = c_{hex} = c_{subcell} = 16.36$ Å) resulting from the crystal structure investigation of $Yb_2Al_{15}Pt_6$. It may be noted that the superstructure reflections were clearly detectable in all of the powder patterns, independently of the starting component ratio, as well as of the presence of minority phases in the products. To check for a possible deviation of the unit cell parameters a_{orth} and b_{orth} from the "ideal" ones for an ortho-hexagonal lattice ratio of $\sqrt{3}$, a diffraction experiment using synchrotron radiation was performed (Fig. 2). Comparing the full width at the half maximum (FWHM) of the *hkl* reflections with those of the 00*l* series (*e.g.* 008) we did not detect any broadening or splitting within the resolution limits of the synchrotron diffraction data. From this experiment we can conclude that the orthorhombic structure of $Yb_2Al_{15}Pt_6$ possesses an "ideal" ortho-hexagonal unit cell with an a_{orth}/b_{orth} ratio of $\sqrt{3}$, in good agreement with the local trigonal symmetry of the slabs *A* and *B* [6]. Similar observations were already made for $Y_2Ga_9Co_3$ [5]. The lattice parameters of $Yb_2Al_{15}Pt_6$ were refined from the diffraction angles of 217 reflections, extracted by profile fitting of the synchrotron powder pattern ($\lambda = 0.495883$ Å, $3.40^o < 2\theta < 39.60^o$). Due to the fact that the positions, as well as the intensities, of most of the reflections (with the exception of the 00*l* series) are perfectly superposed with others, proper indexing of the powder diffraction pattern requires taking into consideration the contribution of each reflection to the observed diffraction peak. Therefore, for the determination of the lattice parameters, the diffraction angles of the observed peaks were used twice, or even thrice with different *h*, *k*, *l* indexes. In this manner the number of used reflection positions was increased to 461 and the lattice parameters were refined to $a = 12.7969(1)$ Å, $b = 7.38813(7)$ Å and $c = 16.3605(2)$ Å, $a/b = 1.73209$. The formula unit volume of $Yb_2Al_{15}Pt_6$ fits to the contraction reported for the rare-earth series $RE_2Al_{15}Pt_6$ [1] (Fig. 3), indirectly indicating a predominant $4f^{13}$ electronic configuration for the Yb atoms (Yb^{3+}), in agreement with the results of the study of physical properties [21].

Crystal structure solution and refinement

Automatic indexing of the collected single-crystal data revealed a hexagonal unit cell with lattice parameters $a_{hex} = 7.38$ Å and $c_{hex} = 16.36$ Å. However, a careful examination of the reflection intensities revealed a rather large value of $R_{int} = 0.107$ for hexagonal symmetry 6/*mmm*. From the three possible *C*-centered ortho-hexagonal settings, only one showed improved agreement of the reflection intensities: Laue class

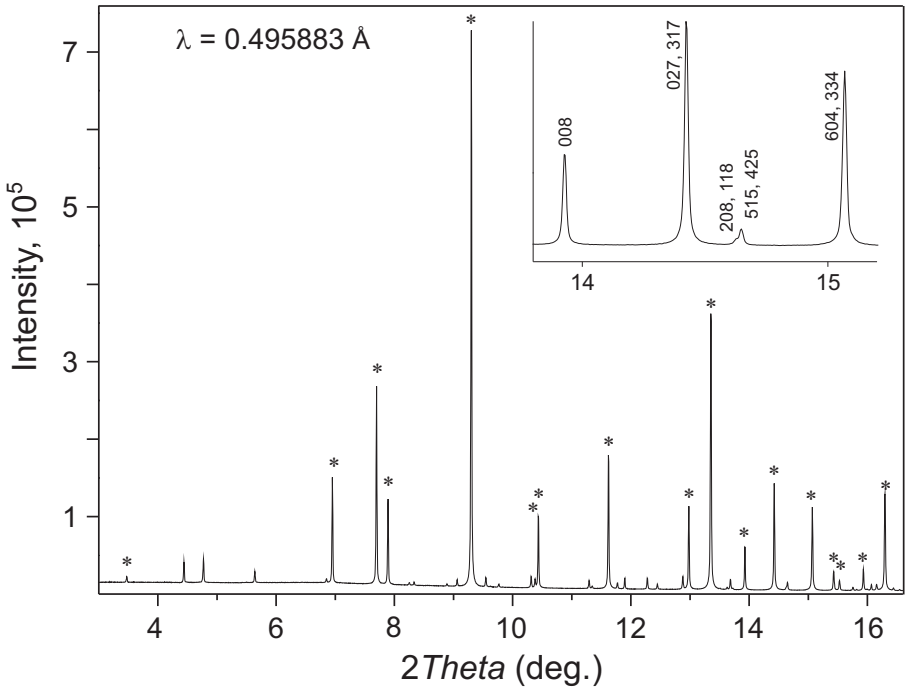

Fig. 2 Synchrotron powder diffraction pattern of $Yb_2Al_{15}Pt_6$. Asterisks mark the reflections that correspond to the $Sc_{1.2}Fe_4Si_{9.8}$ type subcell. The weak reflections belong to the superstructure. The insert shows a comparison of *hkl* reflections with the axial reflection 008: no splitting is observed.

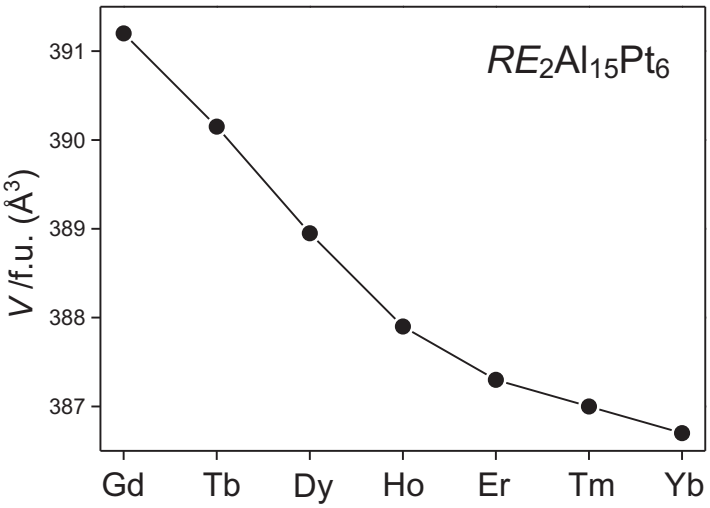

Fig. 3 Volume per formula unit of compounds $RE_2Al_{15}Pt_6$ (*RE* = Gd–Yb).

mmm; transformations: $\mathbf{a}_1 = 2\mathbf{a}_{hex}+\mathbf{b}_{hex}$ $\mathbf{b}_1 = \mathbf{b}_{hex}$, $\mathbf{c}_1 = \mathbf{c}_{hex}$, $R_{int} = 0.089$; $\mathbf{a}_2 = \mathbf{a}_{hex}+2\mathbf{b}_{hex}$, $\mathbf{b}_2 = -\mathbf{a}_{hex}$, $\mathbf{c}_2 = \mathbf{c}_{hex}$, $R_{int} = 0.081$; $\mathbf{a}_3 = \mathbf{a}_{hex}-\mathbf{b}_{hex}$, $\mathbf{b}_3 = \mathbf{a}_{hex}+\mathbf{b}_{hex}$, $\mathbf{c}_1 = \mathbf{c}_{hex}$, $R_{int} = 0.035$. The data set was finally indexed with the latter setting, and the crystal structure was solved in the space group *Cmcm*, which was deduced from the systematic extinction conditions (observed reflections: *hkl* with $h + k = 2n$, *h*0*l* with $l = 2n$). The platinum (Pt1, Pt2) and ytterbium (Yb1) positions were assigned by interpretation of the Patterson function; all the aluminum atoms were located from difference Fourier maps. A structure refinement with anisotropic displacement parameters for all of the atoms rapidly converged and resulted in the residuals $R1 = 0.037$ and $wR2 = 0.079$. The difference Fourier synthesis of this refinement evidenced a small peak

(4.85 e/Å^3) at a 4*c* site (0, 0.82, ¼), which is very close to Al3 and Al6 positions (~1.5 Å). This is caused by a negligible disorder in the relative arrangement of the layers *A* (see discussion below). To describe this position (Yb2), the scattering factor of Yb was used and the occupancy was constrained with that of Yb1, while the isotropic atomic displacement parameter (U_{iso}) was fixed at the value of U_{eq} obtained for Yb1. This slightly reduced the residuals ($R1 = 0.036$ and $wR2 = 0.073$) and resulted in an occupancy ratio of Yb1 : Yb2 = 0.987(2) : 0.013. Since the occupancy factor of the Yb2 position is very small, we will disregard this site in the following structure description and consider that the structure of $Yb_2Al_{15}Pt_6$ is completely ordered.

Description of the structure of $Yb_2Al_{15}Pt_6$

The crystal structure of $Yb_2Al_{15}Pt_6$ is formed by nine crystallographically independent positions (disregarding the small disorder of Yb): one for Yb, two for Pt and six for Al atoms (Table 2). Each ytterbium atom has a regular environment consisting of 11 Al and 6 Pt atoms. It is sandwiched between two corrugated Pt_3Al_3 hexagons with Yb–Al and Yb–Pt contacts of about 3.11 Å and 3.34 Å, respectively. The coordination polyhedron of ytterbium is completed by three Al atoms located within the same layer *A* as the central atom (d(Yb–Al) = 3.04 Å), and two Al atoms situated on the pseudo-trigonal axis, above and below the hexagons (d(Yb–Al) = 3.33 Å). The Al atoms around Yb are located at the vertices of an *Edshammar* polyhedron (CN = 11 [40]). The shortest distance of 4.26 Å between two Yb sites is appreciably longer than the interatomic distance of 3.88 Å, found for elemental Yb (*fcc*, CN = 12) [41]. The nearest environment of each Pt atom has the shape of a distorted cube and is exclusively formed by Al, with two additional Yb atoms opposite adjacent faces. The Pt–Al distances, $d(n')$, cover a relatively large range from 2.478 to 2.726 Å, indicating the presence of empirically different Pt–Al interactions in the structure. The corresponding bond orders n, calculated by the formula $d(n') = d(1) - 0.71 \log(n)$, using a single-bond distance of $d(1) = r(\text{Pt}) + r(\text{Al}) = 1.295 + 1.248 = 2.543$ Å, vary between 1.23 and 0.55 [42]. Using the same argumentation and comparing the shortest Pt–Pt distances of 4.211 Å with the value of 2.770 Å, observed in elemental Pt [43], we can exclude homonuclear Pt–Pt interactions in the structure of $Yb_2Al_{15}Pt_6$. The coordination numbers of aluminum are 10 and 11. The Al1 and Al4 sites have nearly identical environments, with four closest contacts to platinum and six to aluminum atoms, located at the apexes of a tetrahedron and an octahedron, respectively. To the coordination environment of Al1 belongs additionally one Yb atom, located on the pseudo-threefold axis. Similarly, the coordination environments of Al2 and Al5, as well as of Al3 and Al6, are identical two by two, due to the local trigonal symmetry of the slabs *A* and *B*. The Al2 (Al5) atoms are located in-between corrugated Pt_3Al_3 hexagons and planar Yb_2Al_2 quadrangles. The coordination polyhedron of the Al3 (Al6) atom is a distorted Yb_2Al_6 cube completed by 2 Pt atoms. Most of the Al–Al distances vary between 2.821 and 2.896 Å, with the exception of the rather short distances of 2.636 and 2.649 Å within the triangular Al_3 cluster in the layer *A*. In view of the interatomic distance of 2.863 Å in elemental aluminum (*fcc*, CN = 12, [41]), all the observed distances should reflect bonding interactions.

A projection of the crystal structure of $Yb_2Al_{15}Pt_6$ along the shortest translation period, *b*, is shown in the upper part of Fig. 4. The structure is depicted as stacking of the two kinds of slab, *A* and *B*, mentioned in the introduction (Fig. 1). The slabs are stacked along [001] in the sequence $(ABB)_2$. The slabs of type *A* are perfectly planar, thus they are called layers. Within the unit cell they have the composition Yb_4Al_6 and may be understood as a honeycomb-like arrangement of Yb atoms, and triangular Al_3 units located at the center of each condensed Yb_6 hexagon. Disordered variants of such layers have been found in the crystal structures of several gallium compounds $YbGa_{2.63}$ [43], $Eu_{1-x}Ga_{2+3x}$ [44], $Eu_{3-x}Ga_{8+3x}$ [45], $Sr_{3-x}Ga_{8+3x}$ [46], $Ca_{1-x}Ga_{2+3x}$ [47] and $Sr_{1-x}Ga_{2+3x}$ [48]. The slabs of type *B* have the composition Pt_6Al_{12} and can be understood as strongly puckered layers, distorted in such a way that the aluminum atoms coordinate platinum in octahedral manner. The octahedrons are strongly compressed along [001] and are interconnected in the slab by sharing edges. Both slab *A* and *B* possess trigonal symmetry. While the threefold axes of the slabs *B* coincide in the crystal structure of $Yb_2Al_{15}Pt_6$, the relative arrangement of layers *A* violates trigonal symmetry for the whole structure, as first found for $Y_2Ga_9Co_3$ [6]. The projection of two adjacent layers *A* along the stacking direction [001] is represented in the lower part of Fig. 4. This figure clearly demonstrates that the structure of $Yb_2Al_{15}Pt_6$ is truly orthorhombic, even if the building slabs *A* and *B* possess nearly perfect trigonal symmetry and the ratio of the lattice parameters a_{orth}/b_{orth} is practically equal to $\sqrt{3}$.

Related structures

The crystal structure of $Yb_2Al_{15}Pt_6$ represents an ordered variety of the $Sc_{1.2}Fe_4Si_{9.8}$ aristotype [5]. The ordered arrangement of the building blocks leads to reduction of the symmetry from hexagonal, observed for the $Sc_{1.2}Fe_4Si_{9.8}$ type subcell, to orthorhombic for the title compound. A rather large number of compounds of silicon, aluminum and gallium [1-5,8-20], reported over the last three decades, belong to the $Sc_{1.2}Fe_4Si_{9.8}$ family. They have similar hexagonal lattice parameters ($a \sim 4$ Å, $c \sim 16$ Å) and $(ABB)_2$ stacking sequence of two-dimensionally infinite atomic slabs *A* and *B* as building blocks, similar to those just discussed for $Yb_2Al_{15}Pt_6$.

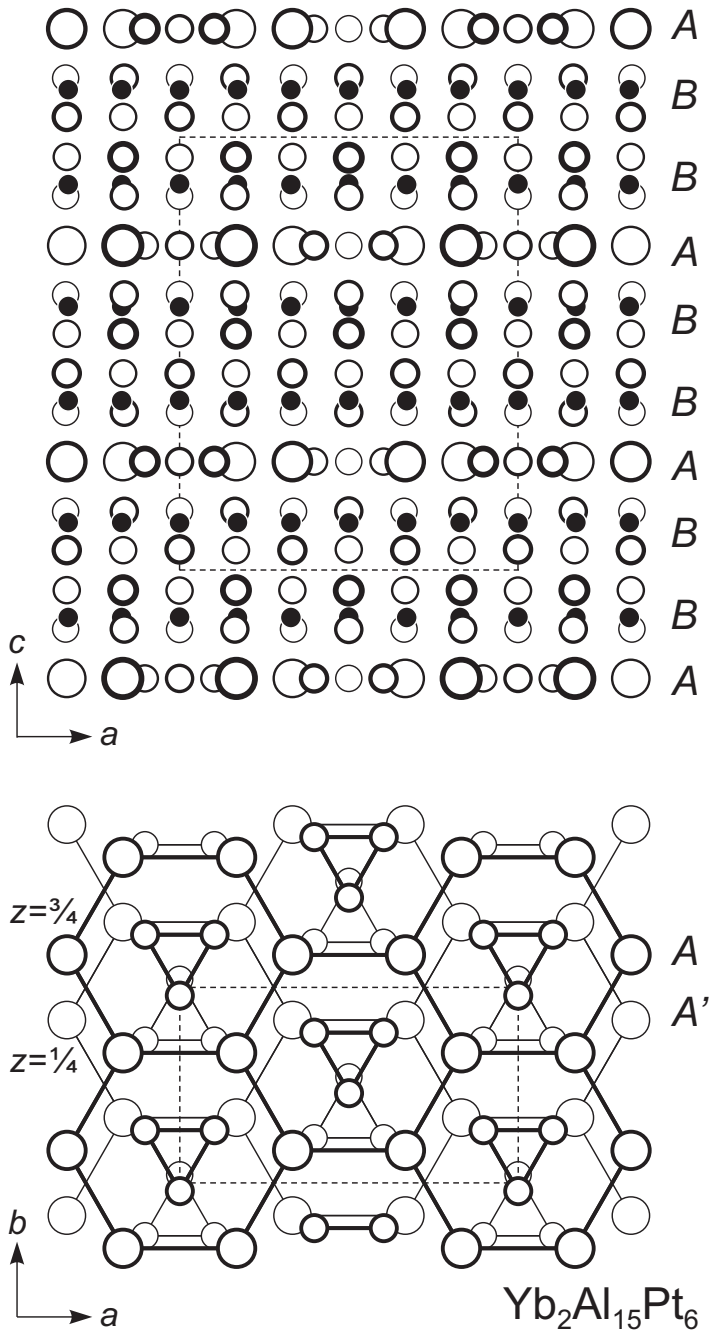

Fig. 4 Crystal structure of $Yb_2Al_{15}Pt_6$: (top) projection along the crystallographic *b* axis; (bottom) relative arrangement of layers *A*. The structure consists of slabs *A* and *B*, similar to those shown in Fig. 1.

Oppositely to $Yb_2Al_{15}Pt_6$, the layers *A* for the other representatives of the $Sc_{1.2}Fe_4Si_{9.8}$ family are in the previous studies described with partial occupancies of about ⅔ and ⅓ for the largest atoms in the structure, usually a rare-earth element (*RE*), and the main group elements (*M*), respectively. Due to the disordered description of the layer *A* and different interpretation of the disorder, the composition of these compounds is represented by different formulas, so that the assignment of the reported structures to the $Sc_{1.2}Fe_4Si_{9.8}$ type is sometimes not obvious (see Table 4 for a summary of literature data).

Mainly two scenarios for the disorder in the layers *A* are discussed in the literature. According to the first one the disorder within the layers *A* is caused by the random replacement of *RE* species by triangular M_3 clusters [5,12], in other words M_3 triangles are statistically distributed within the hexagonal mesh of *RE* atoms. In the second interpretation, the layers *A* are completely ordered but randomly arranged along

Table 4 Composition of ternary and quaternary compounds with the $Sc_{1.2}Fe_4Si_{9.8}$ type of crystal structure. The composition in the second column is normalised to 6 atoms of the transition element in the formula unit.

Reported composition	Normalized composition	Literature
$RE_{1.2}Fe_4Si_{9.8}$	$RE_{1.8}Fe_6Si_{14.7}$	*RE* = Sc [5], Gd [18], Dy [19], Er [17]
$RE_{1.2}Fe_4Si_{9.9}$	$RE_{1.8}Fe_6Si_{14.85}$	*RE* = Y, Gd–Lu [11]
$RE_2Fe_4Si_9$	$RE_3Fe_6Si_{13.5}$	*RE* = Gd–Lu [13]
$U_{1.2}Fe_4Si_{9.7}$	$U_{1.8}Fe_6Si_{14.55}$	[16]
$RE_{0.67}Ni_2Ga_{5+n-x}Tt_x$	$RE_2Ni_6(Ga,Tt)_{15+3n}$	*RE* = Y, Sm, Ho, *Tt* = Ge [8]
		RE = Tb, *Tt* = Si [8]
$Sm_{0.67}Pd_2Al_5$	$Sm_2Pd_6Al_{15}$	[4]
$U_{2/3}Pd_2Al_5$	$U_2Pd_6Al_{15}$	[20]
$RE_{1.33}Pt_4Al_{10}$	$RE_2Pt_6Al_{15}$	*RE* = Zr, Y, Gd–Tm [1]
$RE_{0.67}Pt_2Al_5$	$RE_2Pt_6Al_{15}$	*RE* = Ce [10], *RE* = Tb [3], *RE* = Sm [4]
$Gd_{0.67}Pt_2(Al, Si)_5$	$Gd_2Pt_6(Al,Si)_{15}$	[9]
$U_{1-x}Pt_2Al_{7-6x}$	$U_{3-3x}Pt_6Al_{21-18x}$	[12]
$Ce_{2-x}Pt_4Ga_{8+y}$	$Ce_{3-1.5x}Pt_6Ga_{12+1.5y}$	[14]
$Ce_2Pt_6Ga_{15}$	$Ce_2Pt_6Ga_{15}$	[15]

the crystallographic *c* direction [9,10]. We prefer the latter model as a plausible explanation of the disorder in the structures of the $Sc_{1.2}Fe_4Si_{9.8}$ type. It is supported by the fact that routinely a nearly constant *RE*:*M* ratio of 2:1 is observed within the layers *A*. Additional arguments for this scenario is the diffuse scattering along *c** recorded on electron and X-ray diffraction patterns [1,8,10,15], indicating distorted and incoherent periodicity along [001]. Negligible faults in the relative arrangement of the layers *A* were present also in the single crystal specimen investigated here. This became apparent through a small, but well defined, peak on the difference Fourier maps (very close to the Al3 and Al6 positions, *cf.* section *Crystal structure solution and refinement*). The location of this peak at the center of the Al_3 triangle exactly corresponds to the location of the partially occupied *RE* atoms in the average model of the $Sc_{1.2}Fe_4Si_{9.8}$ type. The expected positions of Al atoms around the Yb1 site could not be localized on the difference Fourier maps due to the marginal degree of such structure faults of about 1.3(2) % and the small scattering power of aluminum.

To understand the reason of this disorder we should examine the nearest environment of *RE* atoms and M_3 triangles. Layers *A* are sandwiched between slabs *B* so that the *RE* atoms and M_3 triangles have nearly identical coordination in the form of two corrugated T_3M_3 hexagons (Fig. 5). On the other hand, for the ordered description of the layer *A* one has to use a hexagonal mesh with a 3 times larger area than that used for the description of the slab *B*. As a consequence, the *RE* atoms or M_3 triangles have three alternative possibilities to be positioned between slabs *B*, opposite the centers of the T_3M_3 hexagons, practically without change of their nearest environment (*A*1, *A*2 and *A*3 in Fig. 1). Evidently, the large *A*–*A*-layer separation of ~8 Å results in a too low driving force for long-range ordering in most of the investigated compounds. Additionally, the disorder in the structures of the $Sc_{1.2}Fe_4Si_{9.8}$ type may also be caused by deviation from optimal conditions during the sample preparation (*e.g.* initial ratio of the starting components, annealing temperature, duration of the thermal treatment, applied crystal growth methods, *etc*.).

The topology of the individual slabs *A* and *B* described for $Yb_2Al_{15}Pt_6$ is the same as found in the related structures of $Y_2Ga_9Co_3$ (space group *Cmcm*) [6], $Yb_2Ga_9Pd_3$ (space group $P6_122$) [49,50], $Tb_2Ge_3Pt_9$ (space group *C*2/*c*) [51] and $Er_4Al_{24}Pt_9$ (space group *P*-1 [7], note that the transition metal and main group elements in $Tb_2Ge_3Pt_9$ are interchanged with respect to the other compounds). First of all, the structures of the $Y_2Ga_9Co_3$ family differ by the ratio and the stacking sequence of the slabs *A* and *B*, which is directly reflected in their nominal compositions. In the compounds with composition 2:3:9, the slabs *A* and *B* alternate in the ratio 1:1. To complete the translation period, the ordered sequence is described by four slabs, according to $(AB)_2$, in the structures of $Y_2Ga_9Co_3$ and $Tb_2Ge_3Pt_9$, and by twelve slabs, as $(AB)_6$, in $Yb_2Ga_9Pd_3$. In the structure of $Er_4Al_{24}Pt_9$ the stacking sequence is *ABBAB*. The latter example combines the ordering sequences observed in the structure reported for $Yb_2Al_{15}Pt_6$ and in the phases with composition 2:3:9. Furthermore, the discussed structures possess different symmetries (even for identical compositions, as in the case of the 2:3:9 series), which arise through the relative arrangement of the individual slabs, namely the layers *A*. The pseudo-trigonal axes of the slabs *B* coincide in the discussed structures and – as a consequence – their relative alignment does not have any influence on the symmetry.

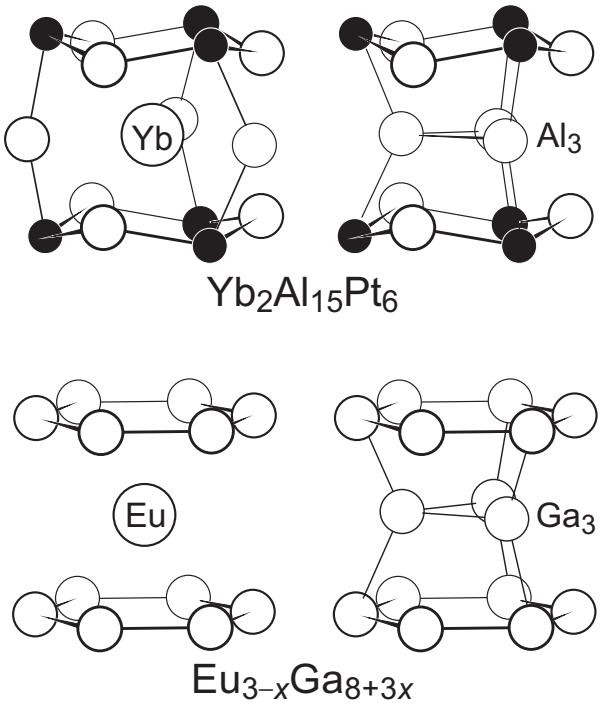

Fig. 5 Coordination of the Yb atoms and Al_3 groups in the structure of $Yb_2Al_{15}Pt_6$, compared with the environment of the Eu atoms and Ga_3 groups found in the structures of $Eu_{1-x}Ga_{2+3x}$ and $Eu_{3-x}Ga_{8+3x}$.

The crystal structures of $Yb_2Al_{15}Pt_6$, $Y_2Ga_9Co_3$, $Yb_2Ga_9Pd_3$, $Tb_2Ge_3Pt_9$, and $Er_4Al_{24}Pt_9$ are shown in Fig. 6 as projections of the layers *A* along their pseudo-trigonal axes. For better visualization, only the triangular M_3 clusters are sketched. The simplest examples in this series are $Y_2Ga_9Co_3$ and $Yb_2Al_{15}Pt_6$, where only two different orientations of the triangular M_3 units are present. While in $Y_2Ga_9Co_3$ pairs of triangles have adjacent edges, the pairs of Al_3 clusters in the projection of $Yb_2Al_{15}Pt_6$ overlap by single vertices. The projections of both structures, $Yb_2Ga_9Pd_3$ and $Tb_2Ge_3Pt_9$, show a hexagonal motif. But only the structure of $Yb_2Ga_9Pd_3$ is truly hexagonal with the triangular Ga_3 units arranged around a hexagonal screw axis, which is running through the origin of the unit cell. Within the unit cell, the Ga_3 clusters are located around 3_1 axes. In contrast, the Pt_3 units in $Tb_2Ge_3Pt_9$ are not related by any hexagonal (or trigonal) axis. They are stepwise shifted along the base of the triangles, resulting in monoclinic symmetry of the crystal structure. The motif of M_3 clusters in the projection of the triclinic structure of $Er_4Pt_9Al_{24}$ consists of both adjacent and overlapping triangles.

As the examples show, the notation used up to now for the discussed compounds, consisting of the character sequence of the building blocks *A* and *B*, describes the stoichiometry, but does not completely reflect the structural particularities. This is especially noticeable for the structures of $Y_2Ga_9Co_3$ and $Tb_2Pt_9Ge_3$, which are described by four slabs in the sequence *ABAB*, but possess different relative arrangements of the slabs *A*. We have tried to improve the notation by accounting for the relative orientation of the *A* slabs in the sequence. As basis for this description we use the two simplest ordering variants of slabs *A*, observed in the structures of $Y_2Ga_9Co_3$ and $Yb_2Al_{15}Pt_6$, schematically represented in their projections along the pseudo-trigonal axes as triangles with adjacent edges and overlapping vertices, respectively (Fig. 6). An analysis of the peculiarities of the discussed structural family showed that “edge” and “vertices” settings occur if the neighboring layers *A* are separated by one and two slabs of type *B*, respectively. The relative orientation of the triangles located in neighboring layers *A* is described in the trigonal coordinate system by the basic vectors ***a*** and ***b*** (Fig. 6), which reflect the pseudo-trigonal symmetry of the individual blocks. Starting from a randomly selected triangle of the slab A_1, one moves stepwise to the following slabs *A* (A_2, A_3, A_4 ...) and notes the relative location (expressed by the corresponding vector) of the triangle M_3 in the slab. The first step defines the direction of the vector ***a***, in other words the first step defines the orientation of the trigonal coordinate system. In this notation the ordering sequences in the structures $Y_2Ga_9Co_3$ and $Yb_2Al_{15}Pt_6$ are represented as $A^{(a)}BA^{(-a)}B$ and $A^{(a)}BBA^{(-a)}BB$, respectively (Fig. 6). Using this approach we can describe the ordering sequences in the structures discussed above as $A^{(a)}BA^{(a+b)}B$ for $Tb_2Ge_3Pt_9$, $A^{(a)}BA^{(a+b)}A^{(b)}BA^{(-a)}BA^{(-a-b)}BA^{(-b)}B$ for $Yb_2Ga_9Pd_3$, and $A^{(a)}BA^{(-a-b)}BB$ for $Er_4Ge_{24}Pt_9$ (Fig. 6).

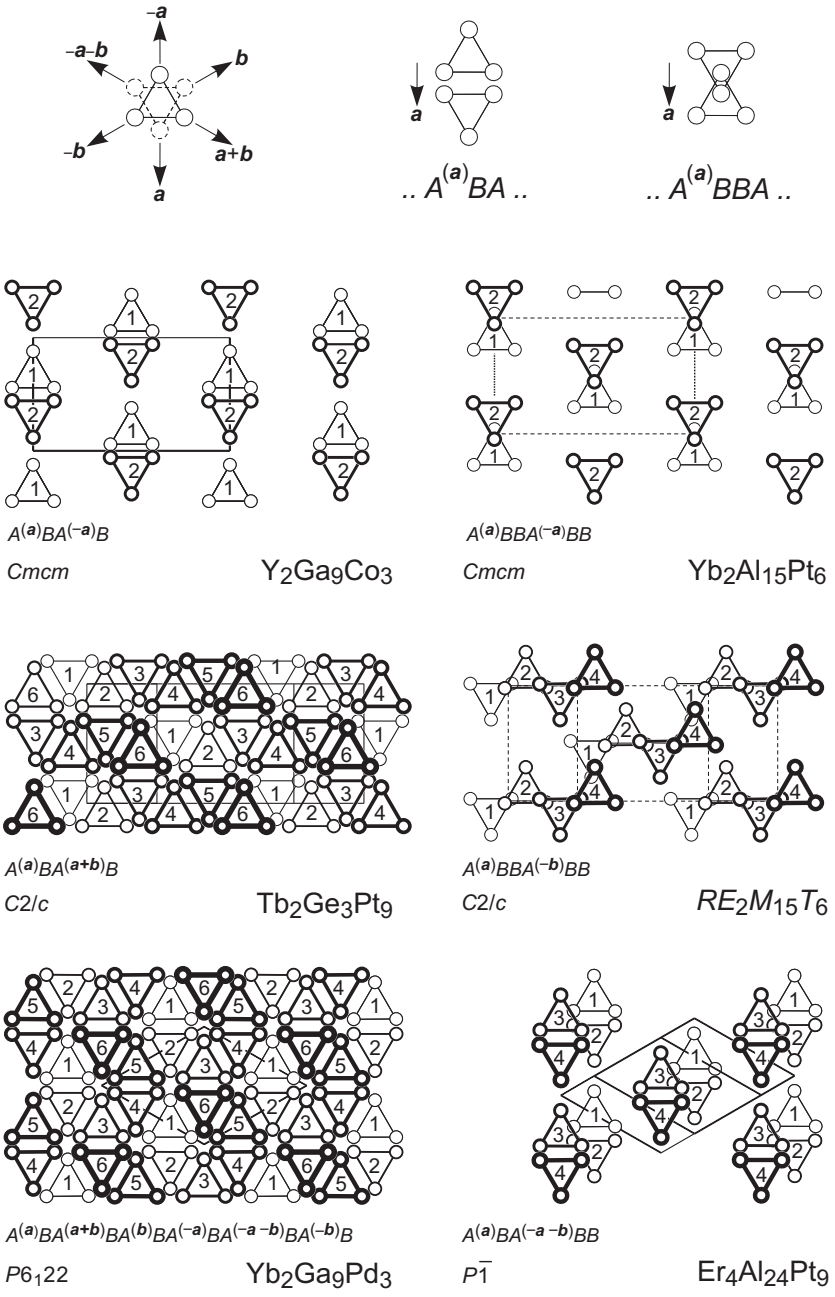

Fig. 6 Stacking of slabs *A* in the related structures of $Y_2Ga_9Co_3$, $Yb_2Ga_9Pd_3$, $Yb_2Al_{15}Pt_6$, $Tb_2Ge_3Pt_9$, $Er_4Al_{24}Pt_9$, as well as in a hypothetical structure $RE_2M_{15}T_6$ (space group *C*2/*c*): (top) basic arrangements used for the description of the ordering sequences of slabs and the set of vectors used for labeling of their relative arrangement; (bottom) stacking sequences of the constituent slabs *A* and *B* in the structures of the $Y_2Ga_9Co_3$ family. Only the triangular units, which correspond to Al_3 clusters in the $Yb_2Al_{15}Pt_6$ structure type, are shown.

The structure model of $Sc_{1.2}Fe_4Si_{9.8}$ reflects an average description of randomly arranged trigonal layers *A*. It should be mentioned that ordering in the structures reported with the $Sc_{1.2}Fe_4Si_{9.8}$ type atomic arrangement (Table 4) would not necessarily lead to the structure of $Yb_2Al_{15}Pt_6$. By analogy with the series of related structures with the $(AB)_n$ sequence ($Y_2Ga_9Co_3$, $Yb_2Ga_9Pd_3$, $Tb_2Ge_3Pt_9$), different ordering varieties may be developed. The simplest alternative model with the same unit cell volume as found for $Yb_2Al_{15}Pt_6$ is obtained if adjacent layers *A* slide stepwise along the base of the triangles (space group *C*2/*c*). The ordering sequence in the resulting structure is $A^{(a)}BBA^{(a+b)}BB$ (Fig. 6). The unit cells of the models with symmetry of the space groups *Cmcm* and *C*2/*c* are related by the following matrix: 1 0 0 0 1 0 ⅓ 0 1;

$a_{mon} = a_{orth} = 12.79$ Å, $b_{mon} = b_{orth} = 7.39$ Å, $c_{mon} = \frac{1}{3}a_{orth} + c_{orth} = 16.95$ Å, $\beta_{mon} = 105.1°$. In previous studies [1-3,8-12], several ordered models for $Sc_{1.2}Fe_4Si_{9.8}$-type derivatives have been proposed. Besides the orthorhombic structure with *Cmcm* symmetry [2,3], which is experimentally confirmed in the present study, there exists a possibility of reorganization of the slabs *A* and the formation of a $4a \times 4b \times c$ superstructure caused by the presence of Si_2 dumbbells.

Electronic structure

The total electronic density of states (DOS) and the DOS obtained by subtracting the Yb 4*f* contribution from the total one are shown in Fig. 7. The positive values are for the majority spin and the negative ones for the minority spin. The Yb 4*f* states give rise to very sharp peaks, but the unoccupied minority spin 4*f* state is somewhat broader and very close to the Fermi level. The Yb 4*f* occupancy was calculated to be 13.3, yielding a spin moment of 0.7 μ_B per Yb atom, instead of the expected value of 1 μ_B for an Yb^{3+} ion. The induced spin moments of the other atoms are negligible (less than ~0.005 μ_B). The density of states at the Fermi energy, $N(E_F)$, is 6.05 states eV^{-1} for the spin-up channel, and 39.12 states eV^{-1} for the spin-down channel. The Yb 4*f* contribution to the former is as expected very small, ~0.01 states eV^{-1},

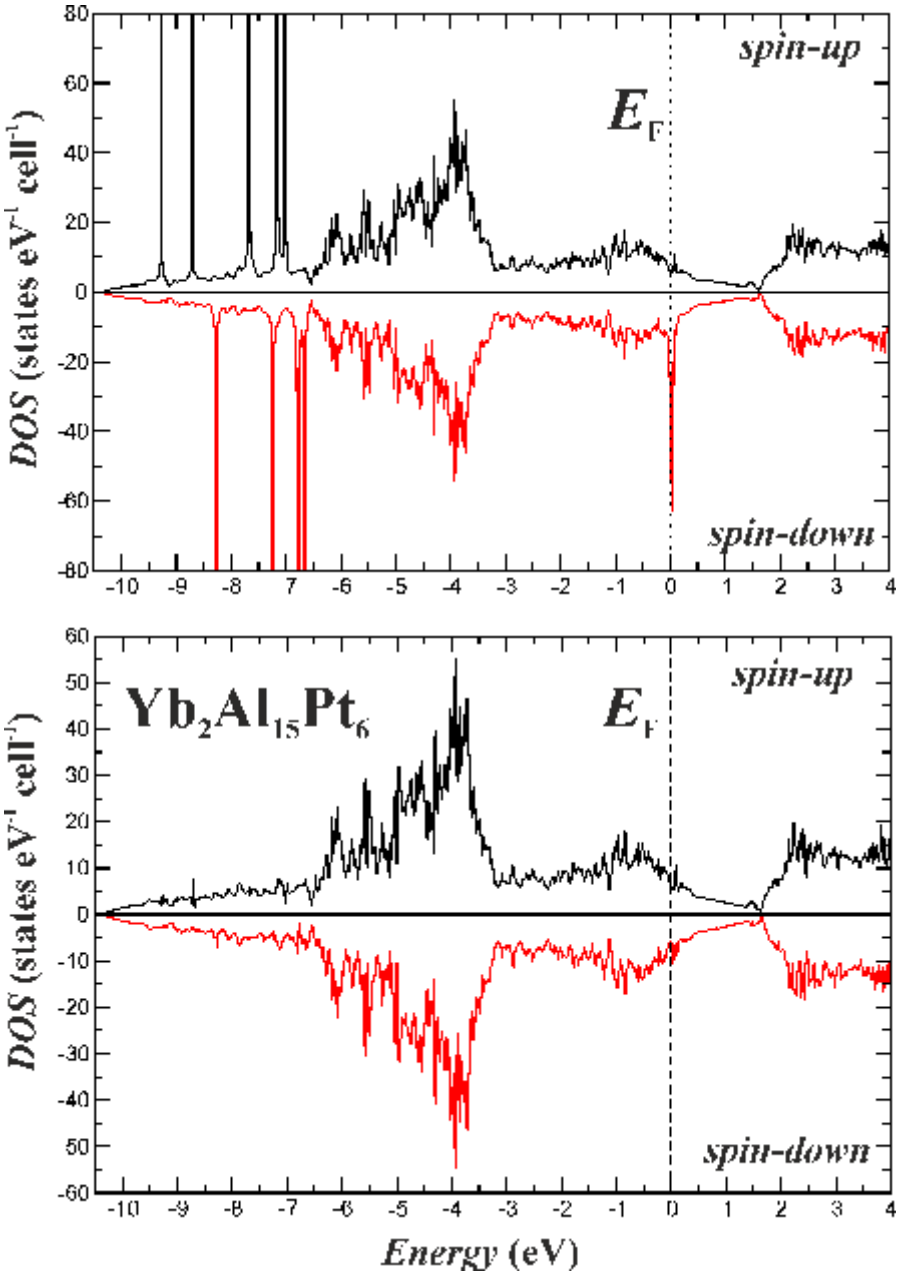

Fig. 7 Calculated electron density of states (DOS) for the completely ordered compound $Yb_2Al_{15}Pt_6$: (top) total DOS for the spin-up and spin-down channels; (bottom) total DOS with subtracted Yb states for the spin-up and spin-down channels.

but very large for the latter, 32.11 states eV^{-1}. The Al 3*s* states contribute significantly between −10.5 and −5.5 eV, the Al 3*p* states start to dominate over 3*s* above −5.5 eV, while the Pt 5*d* states become important in the range between −6.0 and −3.0 eV. The Yb 5*d* contributions remain small in the whole occupied part, with a total occupation value of about 1.4 based on the projected DOS.

The discussion on the crystal structure of $Yb_2Al_{15}Pt_6$ above has already emphasized that the six Al symmetry types have very similar environments in pairs: Al1 and Al4, Al2 and Al5, Al3 and Al6. This similarity also exists in the electronic structure, and applies to the Pt sites as well. This reflects the fact that the orthorhombic unit cell is obtained from an original hexagonal subcell that contains one Pt and three Al sites [1].

The interaction between Pt and Al can be more easily interpreted averaging the Pt1 and Pt2, Al1 and Al4, Al2 and Al5, and Al3 and Al6 contributions. Hybridizations between Al 3*s*,3*p* and Pt 5*d* states are mainly responsible for the atomic interactions between Al and Pt. The Yb 6*s* contributions (not shown) are small and are more or less equally distributed over the whole energy range below the Fermi level, Yb 5*d* contributions below the Fermi level are small. This is characteristic of an ionic interaction of Yb with the Pt–Al substructure.

The ionic contributions to the atomic interactions in $Yb_2Al_{15}Pt_6$ were quantitatively characterized applying the quantum theory of atoms in molecules (QTAIM). In the QTAIM approach the atomic basins are determined from the zero-flux surfaces of the gradient of the electron density. The number of electrons contained in each atomic basin is calculated by integrating the electron density within the corresponding basin: Yb: 68.6 ($Yb^{1.4+}$), Pt1 and Pt2: 81.8 ($Pt^{3.8-}$), Al1: 11.3 ($Al^{1.7+}$), Al4: 11.4 ($Al^{1.6+}$), Al2 and Al5: 11.7 ($Al^{1.3+}$), and Al3 and Al6: 12.2 electrons ($Al^{0.8+}$). We observe that both the Yb and Al atoms lose electrons, and as a result the atomic basins of the Pt atoms hold 3.8 extra electrons. This is in agreement with the electronegativities of the elements. The Al atoms in the flat *A* layers lose somewhat fewer electrons, in comparison with the Al atoms in the *B* layers. This difference can be understood in terms of the different bonding situations for the *A* and *B* layer Al atoms, as revealed by the topological analysis of the electron localizability indicator (ELI).

The coordination of the platinum atoms is relevant for understanding the results of the ELI analysis. The Pt atoms are located in the *B* slabs, and each Pt atom has one Al neighbor from the neighboring *A* layer, another from the neighboring *B* slab, and the remaining six from the same *B* slab. Of the six symmetry independent Al atoms in the crystal structure, two (Al3 and Al6) are in the flat *A* layers, the others in the *B* layers. The shortest Al–Al distances, 2.64 and 2.65 Å, occur within the *A* layer, in the triangle formed by two Al3 atoms and one Al6 atom. The other intra- and interlayer Al–Al distances are longer and range between 2.82 and 2.92 Å.

Despite the fact that geometrically the crystal structure presents itself rather as a layered one, the analysis of the chemical bonding reveals the formation of a three-dimensional framework of covalently bonded Pt and Al atoms (Fig. 8).

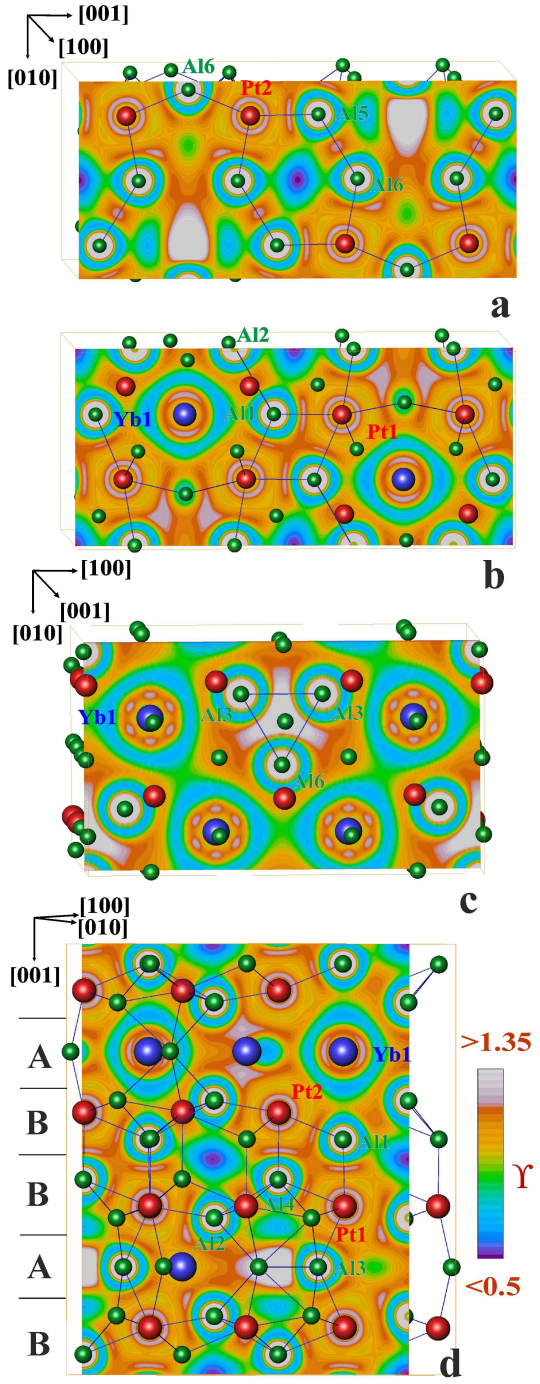

Fig. 8 Electron localizability indicator in $Yb_2Al_{15}Pt_6$: (a) distribution of ELI in the plane at $x = 0.0$; (b) distribution of ELI in the plane at $x \approx 0.83$; (c) distribution of ELI at $z \approx 0.87$; (d) distribution of ELI in the plane of Pt–Al interactions within the slab *B*.

Within the *A* layer, the ELI analysis points out one Al-only bond: the three-center interaction involving the Al3–Al3–Al6 triangle (Fig. 8c). The electron count is 2.6 with the Al3 atoms contributing 0.9 electrons each and Al6 0.8 electrons. Within the *B* slabs different two-center Pt–Al and four-center Pt–Pt–Al–Al bonds are found. In the former the Pt contribution is 2.5 to 3.5 times that of Al (implying highly polar directed bonds). Among the four-center bonds, the Pt1–Pt2–Al2–Al4 type contains 1.1 electrons, with dominant contribution coming from the Pt1 atom (0.5 electrons). To the interaction Pt1–Pt1–Al5–Al4, with an electron population of 0.6, all of the four atoms contribute equally, ~0.15 electrons. The remaining four-center interactions, Pt1–Pt2–Al1–Al2, Pt1–Pt2–Al1–Al5 and Pt1–Pt1–Al1–Al2, have electron populations of around 0.2 each. The covalent interactions between the *A* and *B* layers are in the form of three-center Pt–Al–Al bonds, each containing 1.6 electrons. These bonds are of three types, Pt1–Al2–Al3, Pt1–Al5–Al3 and Pt2–Al2–Al6, where one of the Al participants belongs to the *A* layer (Al3 or Al6) and the two other atoms are from the same *B* layer. The Pt atom contributes 0.9, and each Al 0.3 electrons (the remaining ~0.1 electrons are provided by an Yb atom in the same *A* layer). Two-center highly polar Pt1–Al1 and Pt2–Al4 interactions (Fig. 8d) interconnect two neighboring *B* slabs. The presence of the Al-only bond in the flat layer *A* implies that these Al symmetry types (Al3 and Al6) can keep more electrons, in comparison with the Al types in the *B* layers, because the latter exclusively take part in highly polar covalent bonds with the more electronegative Pt atoms. The Yb atoms were found to participate in some of the Pt–Al bonds, but the number of electrons they contribute is about 5 %, or less, of the total electron population of the bond. The valence shell of Yb (6^{th}) is not present in the ELI distribution, this being a clear indication of charge transfer from Yb to the Pt–Al framework. The structuring of the penultimate shell reveals participation of these electrons (5*d*) in the interactions within the valence region. No direct dative Pt–Yb interactions between the embedded species and the framework, similar to the Au–Ba interactions recently found in the clathrate $Ba_8Au_{5.3}Ge_{40.7}$ [52] or to the Ir–Mg interactions in $Mg_{10}Ir_{19}B_{16}$ [53], were found. Consequently, the Yb interaction with the framework is mostly of ionic nature, a finding being in agreement with the DOS analysis.

Conclusions

The crystal structure of $Yb_2Al_{15}Pt_6$ represents a new structure type of intermetallic compounds. It is an ordered variety of the $Sc_{1.2}Fe_4Si_{9.8}$ aristotype. The structure is described as an $(ABB)_2$ stacking of two trigonal slabs with compositions Yb_4Al_6 (*A*) and Pt_6Al_{12} (*B*). Together with $Tb_2Ge_3Pt_9$, $Yb_2Ga_9Pd_3$ and $Er_4Al_{24}Pt_9$, $YbAl_{15}Pt_6$ belongs to the $Y_2Ga_9Co_3$ family of intergrowth structures formed by different stacking patterns of the slabs *A* and *B*. However, a real-space analysis of the chemical bonding with the electron-localizability approach, showed that the crystal structure is built by an anionic 3D Al–Pt framework, with Yb cations embedded in the cavities. The Al–Pt interaction within the framework is covalent polar, whereas ionic bonding is observed between ytterbium and the framework.

References

[1] J. Nierman, W. Jeitschko, *Z. Anorg. Allg. Chem.* 630 (2004) 361-368.

[2] Yu. Lutsyshyn, Ya. Tokaychuk, V. Davydov, R. Gladyshevskii, *Chem. Met. Alloys* 1 (2008) 303-316.

[3] Yu. Lutsyshyn, Ya. Tokaychuk, R. Gladyshevskii, *Chem. Met. Alloys* 2 (2009) 75-82.

[4] Yu. Lutsyshyn, Ya. Tokaychuk, R. Gladyshevskii, *Chem. Met. Alloys* 5 (2012) 98-102.

[5] B.Ya. Kotur, M. Bruvo, *Sov. Phys. Crystallogr.* 36 (1991) 787-789.

[6] Yu.N. Grin, R.E. Gladyshevsky, O.M. Sichevich, V.E. Zavodnik, Ya.P. Yarmolyuk, I.V. Rozhdestvenskaya, *Sov. Phys. Crystallogr.* 29 (1984) 528-530.

[7] V.M.T. Thiede, B. Fehrmann, W. Jeitschko, *Z. Anorg. Allg. Chem.* 625 (1999) 1417-1425.

[8] M.A. Zhuravleva, X.Z. Chen, X. Wang, A.J. Schultz, J. Ireland, C.K. Kannewurf, M. Kanatzidis, *Chem. Mater.* 14 (2002) 3066-3081.

[9] S.E. Latturner, M.G. Kanatzidis, *Inorg. Chem.* 41 (2002) 5479-5486.

[10] E.V. Murashova, A.I. Tursina, N.G. Bukhan'ko, A.V. Gribanov, I.V. Chernyshev, Yu.D. Seropiegin, *J. Alloys Compd.* 298 (2005) 100-105.

[11] M.-K. Han, Y.-Q. Wu, M. Kramer, B. Vatovetz, F. Grandjen, G.J. Long, G.J. Miller, *Inorg. Chem.* 45 (2006) 10503-10519.

[12] S. Bobev, E.D. Bauer, J.L. Sarrao, *Acta Crystallogr. E* 62 (2006) i77-i79.

[13] E.I. Gladyshevskii, O.I. Bodak, V.I. Yarovets, Yu.K. Gorelenko, R.V. Skolozdra, *Ukr. Fiz. Zh.* 23 (1978) 77-82 (in Russian).

[14] A. Lacerda, P.C. Canfield, W.P. Beyermann, M.F. Hundley, J.D. Thompson, G. Sparn, Z. Fisk, C. Burns, D. Barnhart, A.C. Lawson, G.H. Kwei, J. Goldstone, *J. Alloys Compd.* 181 (1992) 191-196.

[15] G.H. Kwei, A.C. Lawson, A.C. Larson, B. Morosin, E.M. Larson, P.C. Canfield, *Acta Crystallogr. B* 52 (1996) 580-585.

[16] S. Noguchi, K. Okuda, T. Adachi, Y. Haga, E. Yamamoto, Y. Onuki, *J. Phys. Soc. Jpn.* 66 (1997) 2572-2575.
[17] S. Noguchi, K. Okuda, T. Adachi, T. Yoshida, *Physica B* 237-238 (1997) 612-615.
[18] S. Noguchi, T. Sakon, H. Nojiri, M. Motokawa, *Physica B* 346-347 (2004) 183-186.
[19] W. He, L. Zeng, J. Huang, J. Zhang, *J. Alloys Compd.* 458 (2008) 83-87.
[20] Y. Haga, D. Aoki, Y. Homma, S. Ikeda, T.D. Matsuda, E. Yamamoto, H. Sakai, N. Tateiwa, N.D. Dung, A. Nakamura, Y. Shiokawa, Y. Onuki, *J. Optoelectron. Adv. Mater.* 10 (2008) 1601-1606.
[21] M. Deppe, S. Hartmann, M.E. Macovei, N. Oeschler, M. Nicklas, C. Geibel, *New J. Phys.* 10 (2008) 093017.
[22] Yu. Prots, R. Cardoso-Gil, M. Deppe, C. Geibel, Yu. Grin, *Coll. Abstr. XII Eur. Conf. Solid State Chem.*, Münster, September 20-23, 2009.
[23] A. Bergamaschi, A. Cervellino, R. Dinapoli, F. Gozzo, B. Henrich, I. Johnson, Ph. Kraft, A. Mozzanica, B. Schmitt, X. Shi, *J. Synchrotron Radiat.* 17 (2010) 653-668.
[24] R. Bressing, *Acta Crystallogr. A* 51 (1995) 33-38.
[25] STOE WinXPow, Version 2.08, STOE & Cie GmbH, Darmstadt, Germany, 2003.
[26] L.G. Akselrud, Yu. Grin, *J. Appl. Crystallogr.* 47 (2014) 803-805, www.wincsd.eu.
[27] G.M. Sheldrick, *SHELXS-86 – A Program for the Solution of Crystal Structures*, University of Göttingen, Germany, 1986.
[28] E. Parthé, L. Gelato, *Acta Crystallogr. A* 40 (1984) 169-184.
[29] L.M. Gelato, E. Parthé, *J. Appl. Crystallogr.* 20 (1987) 139-143.
[30] K. Koepernik, H. Eschrig, *Phys. Rev. B* 59 (1999) 1743-1757.
[31] V.I. Anisimov, J. Zaanen, O.K. Andersen, *Phys. Rev. B* 44 (1991) 943-954.
[32] J.P. Perdew, Y. Wang, *Phys. Rev. B* 45 (1992) 13244-13249.
[33] H. Eschrig, K. Koepernik, I. Chaplygin, *J. Solid State Chem.* 176 (2003) 482-495.
[34] R.F.W. Bader, *Atoms in Molecules, A Quantum Theory*, Clarendon Press, Oxford, 1995.
[35] M. Kohout, *Int. J. Quantum Chem.* 97 (2004) 651-658.
[36] M. Kohout, F.R. Wagner, Yu. Grin, *Int. J. Quantum Chem.* 106 (2006) 1499-1507;
[37] M. Kohout, *Faraday Discuss.* 135 (2007) 43-54.
[38] A. Ormeci, H. Rosner, F.R. Wagner, M. Kohout, Yu. Grin, *J. Phys. Chem. A* 110 (2006) 1100-1105.
[39] M. Kohout, *Program DGRID*, version 4.6, Radebeul, Germany, 2011.
[40] S. Lidin, Th. Popp, M. Somer, H.G. von Schnering, *Angew. Chem., Int. Ed. Engl.* 31 (1992) 924-927.
[41] J. Donohue, *The Structures of the Elements*, Wiley, New York, 1974.
[42] L. Pauling, *The Nature of the Chemical Bond and the Structure of Molecules and Crystals: an Introduction to Modern Structural Chemistry*, Cornell Univ. Press, Ithaca, NY, 1995.
[43] S. Cirafici, M.L. Fornasini, *J. Less-Common Met.* 163 (1990) 331-338.
[44] O. Sichevych, R. Ramlau, R. Giedigkeit, M. Schmidt, R. Niewa, Yu. Grin, *Coll. Abstr. 13th Int. Conf. Solid Compounds of Transition Elements*, Stresa, Italy, 2000, O-13.
[45] O. Sichevych, Yu. Prots, Yu. Grin, *Z. Kristallogr. - New Cryst. Struct.* 221 (2006) 265-266.
[46] F. Haarmann, Yu. Prots, S. Göbel, H.G. von Schnering, *Z. Kristallogr. - New Cryst. Struct.* 221 (2006) 257-258.
[47] F. Haarmann, Yu. Prots, *Z. Anorg. Allg. Chem.* 632 (2006) 2135.
[48] O. Pecher, F. Haarmann, *Z. Anorg. Allg. Chem.* 634 (2008) 2069.
[49] R. Giedigkeit, W. Schnelle, Yu. Grin, R. Kniep, *Coll. Abstr. VIIth Eur. Conf. Solid State Chem.*, Madrid, 1999, P136.
[50] R. Giedigkeit, *PhD Thesis*, Dresden, 2007.
[51] Yu. Prots, H. Borrmann, W. Schnelle, W. Jeitschko, *Z. Anorg. Allg. Chem.* 631 (2005) 1218-1226.
[52] H. Zhang, H. Borrmann, N. Oeschler, C. Candolfi, W. Schnelle, M. Schmidt, U. Burkhardt, M. Baitinger, J.-T. Zhao, Yu. Grin, *Inorg. Chem.* 50 (2011) 1250-1257.
[53] A.M. Alekseeva, A. Leithe-Jasper, Yu. Prots, W. Schnelle, A. Ormeci, E.V. Antipov, Yu. Grin, *Chem. Met. Alloys* 7 (2014) 74-84.